Acta Geochim (2019) 38(1):159–172
https://doi.org/10.1007/s11631-018-0308-1

ORIGINAL ARTICLE

Jurassic granitoid dike in Luodian, Guizhou Province: discovery and geological significance

Mingjin Zhu[1] · Aiguo Nie[2] · Yazhou Tian[1] · Xinsong Wang[3] · Jun Sun[2]

Received: 26 March 2018 / Revised: 18 October 2018 / Accepted: 23 November 2018 / Published online: 18 December 2018

Abstract In this paper, the Jurassic granitoid dike that intrudes into Permian diabase was reported in Luokun, Luodian County, south Guizhou. Zircon LA-ICP-MS U–Pb dating of the granitoid dike yielded an age of 164.3 ± 2.4 Ma with the εHf(t) range from + 7.8 to + 12.1. The high contents of SiO_2 (65.2%–66.8%) and total alkali ($Na_2O + K_2O$: 9.01%–9.95%), and low contents of Mg, Fe, Ca, P and Ti show the characteristics of alkali-rich granite. The total contents of rare earth elements range from 289.90 to 394.23 ppm. The Rb, Ba, K, Th, U and other LILE, Ta, Sr, P, Ti are enriched, and heavy rare earth elements are depleted. Petrogeochemical characteristics show that the dike was derived from a partial melting of newly-grown basaltic crust, and contaminated by crustal materials before experiencing strong fractional crystallization. The dike was formed in the intraplate post-orogenic extension stage and indicates that parental magma rose to the shallow crust through a fault. This provides new evidence of tectonic and mantle-crust magmatic activities and may contribute to regional Au mineralization in southern Guizhou and neighboring areas.

Keywords Jurassic granitoid dike · Geochemical characteristics · Geochronology · Luodian · Guizhou province

✉ Aiguo Nie
nieaiguo@163.com

[1] Guizhou University, Guiyang 550025, China

[2] Guizhou Institute of Technology, Guiyang 550003, China

[3] State Key Laboratory of Ore Deposit Geochemistry, Institute of Geochemistry, Chinese Academy of Sciences, Guiyang 550002, China

1 Introduction

In Guizhou province, which is mainly covered by sedimentary rocks, igneous rocks are scattered in small areas; examples include the Permian basalts in the west of Guizhou, Late Cretaceous and Permian basic-ultrabasic rocks in the west and south of Guizhou, and the huge granites of the Xuefeng period occurring at the Jiuwandashan area on the border between Guizhou and Guangxi, as well as in Guangxi. Strong epithermal mineralization developed in the west and north of Guizhou, such as Carlin-type Au mineralization (Hu and Zhou 2012), the mineralization age of which spanned largely from 134 to 193 Ma (Chen et al. 2007; Zheng 2017; Liu et al. 2017; Su et al. 2018). Research shows that those mineralization sources may be associated with deep magmatism (Su et al. 2009; Xia et al. 2009; Liu et al. 2017; Xie et al. 2018) but there has been no contemporaneous magmatic event reported in west Guizhou. In recent years, the granitoid dike that intruded in Permian diabase was discovered in Luokun, Luodian County south Guizhou.The petrology, geochemistry, zircon U–Pb dating, and Hf isotope of the dike were analyzed in this paper. The petrogenesis and age of the dike will be very crucial for us to understand the regional mineralization mechanism and tectonic episode.

2 Regional geological setting

The study area is located at the transition zone of the southwest Yangtze Plate and Youjiang Orogenic Belt (Fig. 1a), and belongs to the inner edge of the southwest margin of Yangtze Plate (Wu et al. 1997a, b). The convergence of Yangtze Plate and Huaxia Plate, as well as the accompanied folding and magmatic activity in the

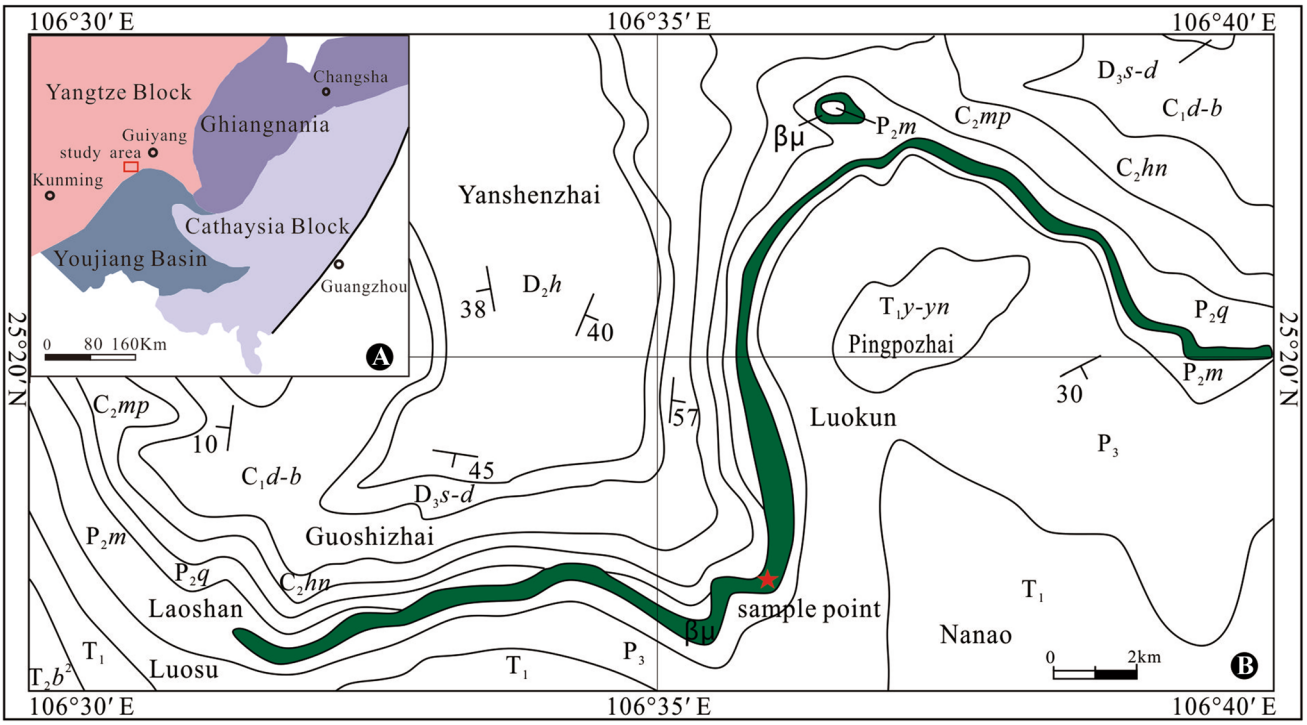

Fig. 1 Geological map of the granitoid (A-modified from Chen et al. 1994; B-modified from the geologic map of Luodian and Leye, 1:200,000). T_2b^2-Midpiece of Bianyang Formation of Middle Triassic; T_1- Lower Triassic; P_2m-Maokou Formation of Middle Permian; P_2q-Qixia Formation of Middle Permian; C_2mp-Maping Formation of Upper Carboniferous; C_2hn-Huanglong Formation of Upper Carboniferous; C_1d-b-Datang-Baizuo Formation of Lower Carboniferous; D_3s-d-Xiangshuidong Formation-Daihua Formation of Upper Devonian; D_2h-Huohong Formation of Middle Devonian; βμ-Diabase

Caledonian period has limited the ancient tectonic framework of this region (Shu 2006).

In Late Paleozoic, basic magmatic activity was widely developed in the middle and northern areas of Guangxi (Wang and Kuang 1997; Zhang et al. 1999; Wu et al. 1993, 1997). Then, in Middle and Late Permian, due to the intense activity of mantle plume and a huge eruption of Emeishan basalt, the extremely thick continental flood tholeiitic basalts accumulated in southwest Guizhou with a maximum thickness of over 2000 m (Xu et al. 2001; Chen et al. 2003). In the late Yanshanian, the lithosphere extended and the accompanied acidic magmatic activity was very intensive in Guangxi, which contributed to the world-class tin polymetallic deposit (Hu and Zhou 2012).

However, in southern Guizhou, the magmatic activity was relatively weak, characterized mainly by the large development of sedimentary rocks in this period. The main strata outcrops in the area are Devonian, Carboniferous, Permian and Triassic sediments, and Permian diabase (Fig. 1b). The diabase mainly emplaces in the limestone of the Middle Permian Maokou Formation as bedrock or dike and locally invades in the Middle Permian Qixia Formation and Upper Carboniferous strata with an inclination angle of 50°–60° and an exposed width of 15–315 m, and usually 100–200 m. The 261.9 ± 2.1 Ma of Zircon SHRIMP dating of the diabase was considered to be the polymorph product of Late Permian Emeishan basalt (Zhu et al. 2018). The granitoid dike cut across the diabase, indicating that it was formed after the Permian.

3 Geological and petrographic characteristics of the granitoid dike

Eight parts can be identified from the section of field outcrop of the granitoid dike (Fig. 2). (1) the normal limestone of P_2m; (2) the marble from the hydrothermal alteration of P_2m limestone, many calcite and quartz veins are in the limestone; (3) fine-grain fresh diabase; (4) coarse-grain fresh diabase; (5) fine-grain diabase with spherical weathering; (6) granitoid dike; (7) altered diabase; the diabese has been altered into clay; and (8) normal limestone of P_2m. The granitoid dike nearly vertically intruded in diabase with an occurrence of 95°∠85° and a width of about 50 cm. The contact between the diabase and the granitoid dike is unambiguous.

Field observations and thin section identification under a microscope have been carried out on the granitoid dike. The rock is pale gray and blocky, and feldspar phenocrysts are visible on hand sample. Phenocrysts that consist mainly

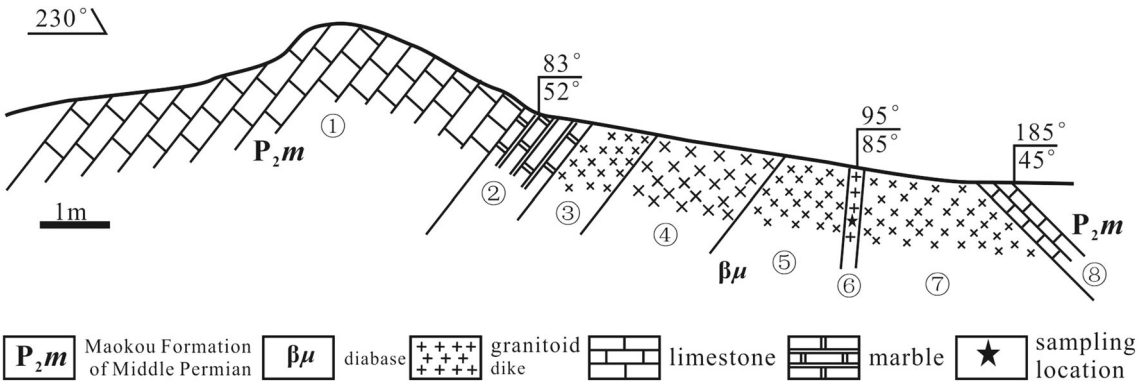

Fig. 2 The cross-section of field outcrop of the granitoid

of plagioclase (70%) and perthite (20%) are mostly rectangular or tabular (Fig. 3a, b) in the porphyritic texture, in which phenocrysts account for about 90% and the matrix accounts for about 10% (Fig. 3c, d). Plagioclase is automorphic or hypautomorphic, uniformly distributed in the plate column shape, and it develops multiple twins with a size of 0.2–3 mm and suffered weak sodium-zoisitization. Perthite is automorphic or hypautomorphic in a thin strip shape with the size of 0.5–1.5 mm. The matrix is composed of biotite (9%) and quartz (1%). Biotite is distributed between the crystals of plagioclase and perthite as the incomplete leaf and fragment shape with the size of 0.02–0.2 mm. We suggest that the plagioclase and perthite were the primary mineral phase during the magmatic process, and the source magma of granitoid was enriched in Na and K. The biotite and quartz were late-magmatic accessory phases, and the zoisite was the product of hydrothermal alteration.

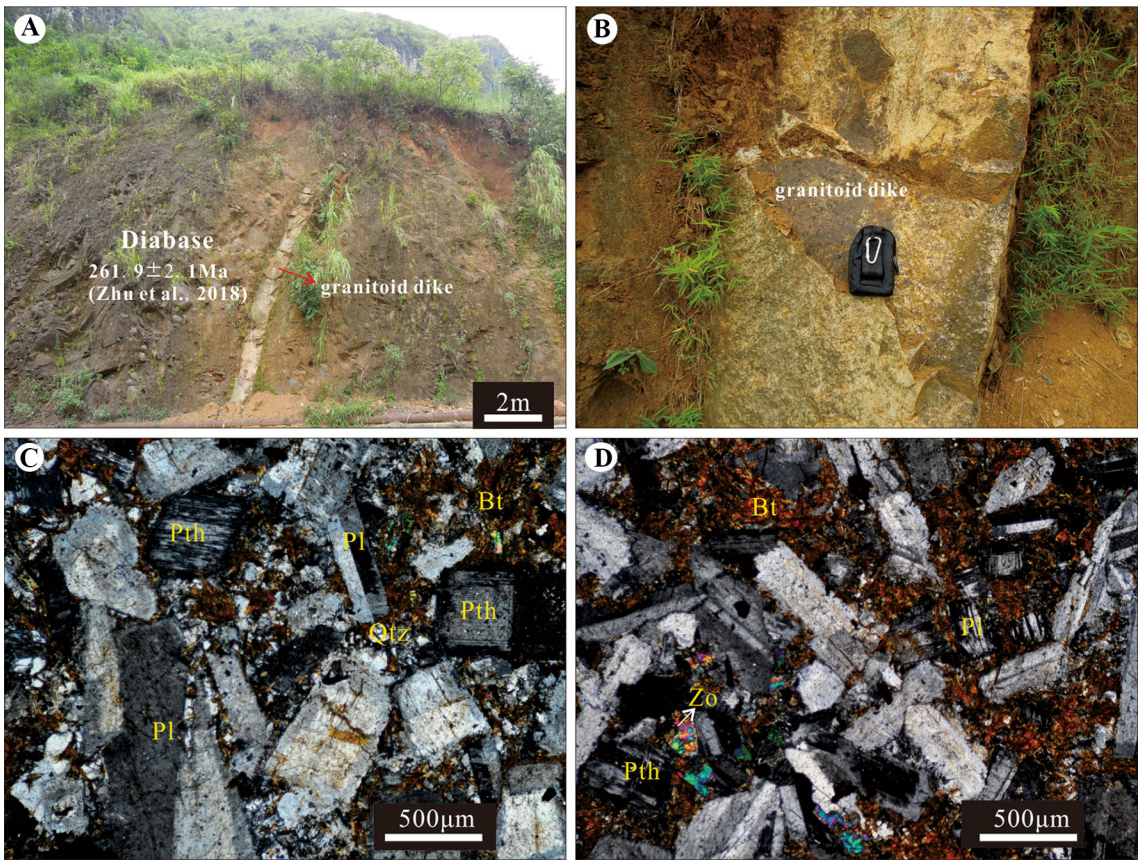

Fig. 3 Features under microscope and field of the granitoid. **a**, **b** Contact relationship between granitoid dike and diabase; **c**, **d** photomicrographs of granitoid (cross-polarized); Qtz-quartz; Pl-plagioclase; Pth-perthite; Zo-zoisite; Bt-biotite

Table 1 Major (wt%) and trace (ppm) element compositions of the granitoid

Samples no.	LK1	LK2	LK2-1
SiO_2	66.8	65.6	65.2
Al_2O_3	15.15	15.45	15.25
$Fe_2O_3^T$	3.54	4.30	4.69
MgO	0.52	0.50	0.56
CaO	1.38	1.73	1.58
Na_2O	5.38	6.60	6.21
K_2O	4.57	2.41	3.00
P_2O_5	0.10	0.20	0.21
TiO_2	0.63	0.78	0.81
MnO	0.09	0.10	0.12
L.O.I.	0.99	1.27	1.31
Total	99.15	98.94	98.94
FeO*/MgO	6.13	7.74	7.54
$Na_2O + K_2O$	9.95	9.01	9.21
A/CNK	0.93	0.93	0.93
Ga	13.35	16.00	15.15
Rb	69.3	37.8	47.9
Ba	1030	600	740
Sr	502	671	531
Zr	600	575	597
Nb	42.5	43.7	45.8
Hf	7.1	7.7	9.0
Ta	1.10	1.24	1.25
Pb	1.1	2.1	2
Th	11.6	10.4	11.3
U	2.1	2.2	2.3
La	56.6	85.7	86
Ce	123.5	165	170.5
Pr	13.2	17.05	17.65
Nd	50.2	62.6	65.1
Sm	10.2	11.85	12.35
Eu	2.59	3.49	3.33
Gd	8.31	10.5	10.95
Tb	1.42	1.68	1.77
Dy	8.96	10.25	10.7
Ho	1.94	2.06	2.19
Er	5.54	5.84	6.2
Tm	0.87	0.86	0.89
Yb	5.67	5.43	5.7
Lu	0.9	0.86	0.9
Y	50.3	57.9	61.7
10000 Ga/Al	1.67	1.96	1.88
δEu	0.83	0.94	0.86
Sr/Y	9.98	11.59	8.61
La/Yb	9.98	15.78	15.09
T (°C)	958	952	956

A/CNK = $(Al_2O_3)/(CaO + K_2O + Na_2O)$ mole fraction ratio; A/NK = $(Al_2O_3)/(K_2O + Na_2O)$ mole fraction ratio; chondrite and primitive mantle data are from Sun and McDonough (1989); $a\delta Eu = Eu_N/[(1/2)(Sm_N + Gd_N)]$; $Fe_2O_3^T$ and FeO* are stand for total iron. T_{Zr} is calculated from zircon saturation thermometry (Watson and Harrison 1983)

4 Samples and analysis method

The samples are located on the side of the road in the southwest of Luokun, Luodian County. Based on detailed field observation of the hypabyssal dike, LK2 was taken from the center of the dike and LK1 and LK2-1 were taken from 20 cm from the center on both sides. All samples were fresh rocks.

The major element, trace element, and rare earth element analysis of three whole-rock samples were completed in the ALS Laboratory (Guangzhou) Co., Ltd. In the major element analysis, the fuse XRF method was adopted for determination and the plasma spectrometry and chemical method were adopted for mutual detection. In the rare earth and trace element analysis, LA-ICP-MS was adopted for testing.

Zircons selection in rocks was conducted in Yuneng Rock and Mineral Separation Technology Service Co., Ltd. in Langfang, Hebei. CL photographs of zircons were taken in the Key Laboratory of Continental Tectonics and Dynamics of Chinese Academy of Geological Sciences. Ziron U–Pb isotopic age and Lu–Hf isotopic analysis were finished with Neptune and other MC-ICP-MS in the isotopic laboratory of Tianjing Institute of Geology and Mineral Resources. A 193 nm excimer laser sampling system (LA-MC-ICP-MS) was adopted for zircon laser ablation. During zircon U–Pb dating, the spot beam of laser ablation was generally 35 μm, the energy density was 13–14 J/cm^2 and the frequency was 8–10 HZ. The laser ablation material was sent to Neptune (MC-ICP-MS) with He as the carrier gas. TEMORA and GJ-1 were taken as the external zircon age standards for U and Pb isotope fractionation correction. The detailed experimental process referred to Geng et al. (2012) and Li et al. (2009a, b). ICP-MS Data Cal program was adopted to make data processing (Liu et al. 2010). ^{208}Pb was used to correct common lead (Anderson 2002) and NIST612 was taken as the external standard to calculate the contents of Pb, U, and Th in zircon samples. Isoplot program was adopted for statistical processing (Ludwing 2001). The error of individual data points was 1σ. $^{206}Pb/^{208}U$ was taken as the age and its weighted average was 95% of confidence level.

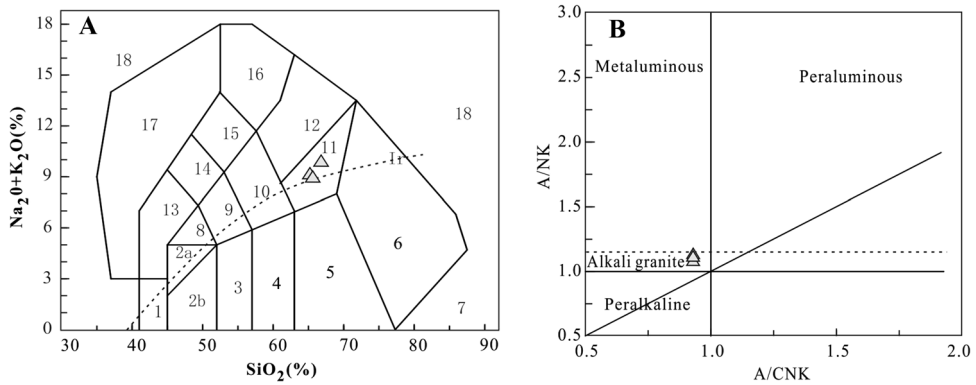

Fig. 4 **a** TAS diagram and **b** A/CNK-A/NK diagram of the granitoid (after Maniar and Piccoli 1989). **a** TAS diagram of granitoid in Luodian; 1-olivine gabbro; 2a-alkali gabbro; 2b- inferior alkali gabbro; 3- gabbrodiorite; 4-diorite; 5-granodiorite; 6-granite; 7-quartzolite; 8-monzogabbro; 9-monzodiorite; 10-monzonite; 11-quartz monzonite; 12-syenite; 13- foid quartz monzogabbro; 14-foid monzogabbro; 15-foid monzosyenite; 16-foid syenite; 17-foid plutionic rock; 18-tawite/urtite/italite; Ir-Irvine alkaline above the boundary line and sub-alkaline below the boundary line; **a**, acidity rock in Luodian A/NK-A/CNK diagram (the base refers to Literature (Maniar and Piccoli 1989); A/CNK = $Al_2O_3/(CaO + Na_2O + K_2O)$, A/NK = $Al_2O_3/(Na_2O + K_2O)$ are all molar ratios

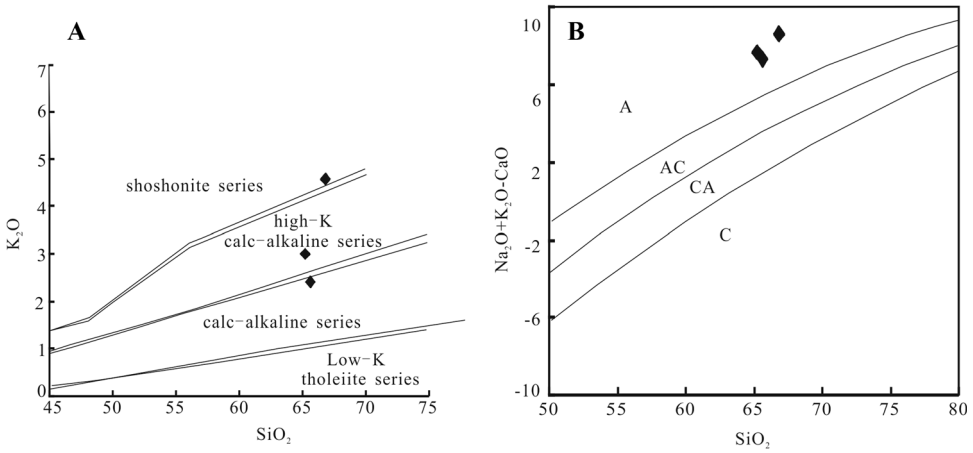

Fig. 5 **a** Si_2O–K_2O diagram of the granitoid (after Peccerillo and Taylor 1976) and **b** (Si_2O–$Na_2O + K_2O$–CaO) diagram of the granitoid (after Frost et al. 2001)

In Lu–Hf isotopic analysis, 8–10 Hz laser frequency, 100 mJ laser intensity, and 50 μm laser beam spot diameter were adopted. Laser ablation material was sent to Neptune with He as the carrier gas. GJ-1 was taken as the monitoring standard sample. In order to make Hf isotopic analysis correspond to zircon U–Pb age analysis, zircon Hf isotopic analysis points and zircon U–Pb age analysis points were located at the same place or structure of the same zircon crystal zone. 1.867 × 10–11/year was used to calculate the decay constant of ^{176}Lu. The ratios of ^{176}Lu to ^{177}Hf and ^{176}Hf to ^{177}Hf of chondrite were 0.0332 and 0.282772, respectively. The ratios of ^{176}Lu to ^{177}Hf and ^{176}Hf to ^{177}Hf of depleted mantle were 0.0384 and 0.28325, respectively. The ratio of ^{176}Lu to ^{177}Hf (average crust) was 0.015. The detailed test process referred Geng et al. (2011).

5 Results

5.1 Rock geochemistry results

The major and trace element data of the whole-rock are shown in Table 1. The rock has high contents of SiO_2 (65.2%–66.8%) and total alkali ($Na_2O + K_2O$: 9.01%–9.95%) and low contents of MgO (0.50%–0.56%), Fe_2O_3 (3.54%–4.69%), CaO (1.38%–1.73%), P_2O_5 (0.10%–0.21%), and TiO_2 (0.63%–0.81%), showing the characteristic of rich alkali granite. In the TAS classification diagram (Middlemost 1994), three samples are all located in quartz monzonite area (Fig. 4a) belonging to the alkaline series, which is consistent with the identification results of lithology. In the A/CNK-A/NK diagram, there are three acidic rock samples. A/CNK ($0.93 \leq 1.0$) belongs to the aluminum alkaline granite (Fig. 4b). Three samples are distributed dispersedly in the Si_2O–K_2O diagram (Fig. 5a), but they all fell into the alkaline series. The main oxides,

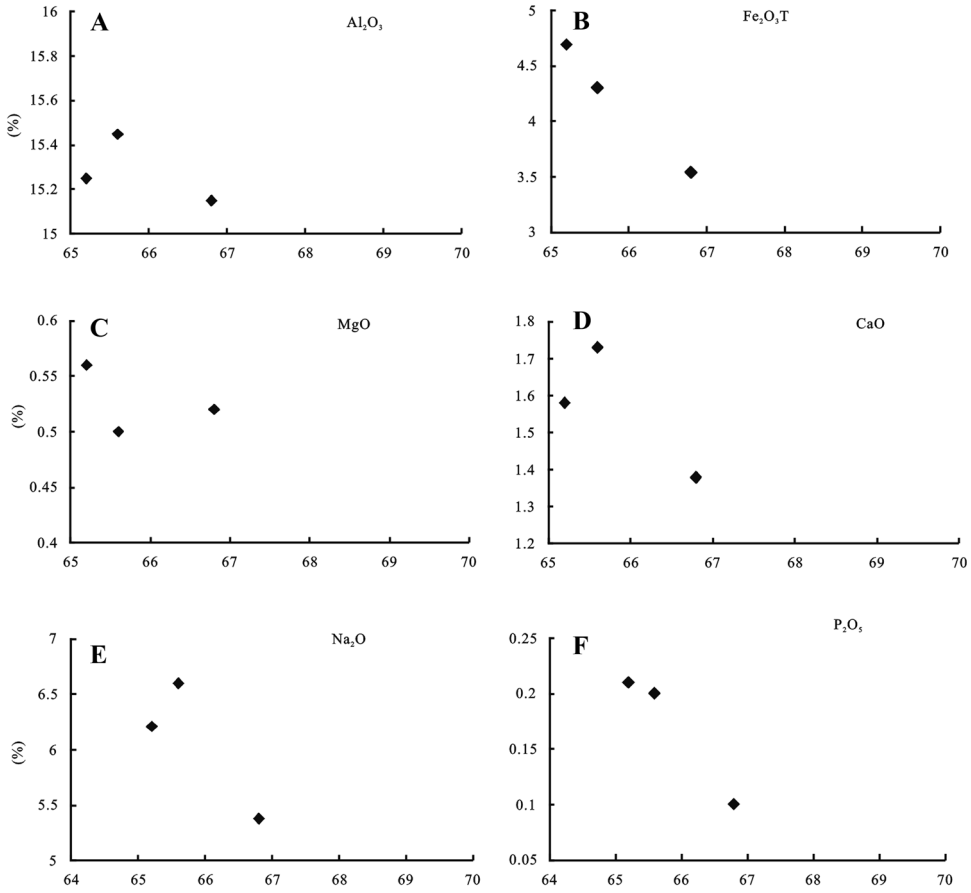

Fig. 6 Harker diagrams for the granitoid

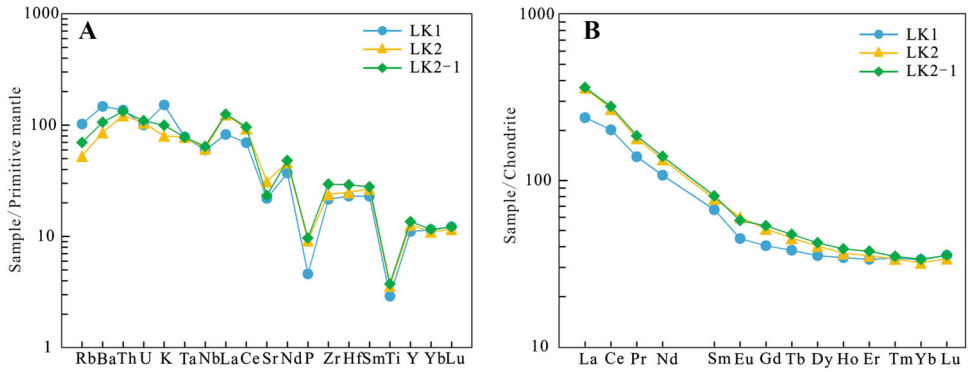

Fig. 7 Primitive mantle-normalized trace element spidergrams (**a**) and chondrite-normalized REE patterns (**b**) diagrams of the granitoid. **a** modified after Sun and McDonough (1989); **b** modified after McDonough and Sun (1995)

Al_2O_3, $Fe_2O_3^T$, MgO, CaO, Na_2O, P_2O_5, are negatively related to SiO_2 in Harker plot (Fig. 6).

The total contents of rare earth elements ranged from 289.90 to 394.23 ppm; La/Yb ranged from 9.98 to 15.78; δEu ranged from 0.83 to 0.94, indicating slight Eu anomaly. The rare earth element distribution map was right-dipping (Fig. 7b), but medium and heavy rare earth elements were relatively flat without significant depletion. According to the trace element spider diagram (Fig. 7a), relative to enriched light rare earth elements, Rb, Ba, K, Th, U, and other LILE, Ta, Sr, P, Ti and heavy rare earth elements depleted. In addition, granitoid in Luodian had relatively low 10,000 Ga/Al (1.67–1.96), FeO*/MgO (6.13–7.74) and Sr/Y (8.61–11.59), and it doesn't show the characteristics of adakitic granite.

5.2 Zircon U–Pb dating result

Zircon U–Pb dating results showed that the $^{206}Pb/^{238}U$ age ranged widely from 2632 to 161 Ma with multiple ranges overall, including 161–168 Ma, 257–280 Ma, 407–499 Ma, 975–1105 Ma, 1405–1520 Ma, ~ 1800 Ma, 2135–2208 Ma, and ~ 2632 Ma (Table 2). It could be seen from CL pictures (Fig. 8) that those zircons had good

Table 2 Zircon U–Pb analytical results for the granitoid

Samples Spot no.	Pb (ppm)	U (ppm)	Th (ppm)	Th/U	$^{207}Pb/^{206}Pb$	± 1σ	$^{207}Pb/^{235}U$	± 1σ	$^{206}Pb/^{238}U$	± 1σ	$^{208}Pb/^{232}Th$	± 1σ	$^{206}Pb/^{238}U$		$^{207}Pb/^{235}U$		$^{207}Pb/^{206}Pb$	
													Age (Ma)	± 1σ	Age (Ma)	± 1σ	Age (Ma)	± 1σ
1	46	576	306	0.5	0.0746	0.0004	0.6723	0.0071	0.0654	0.0007	0.0240	0.0004	464	3	522	6	786	22
2	110	2184	2523	1.2	0.0425	0.0002	0.4537	0.0026	0.0774	0.0004	0.0105	0.0002	268	1	380	2	1132	11
3	41	1190	912	0.8	0.0256	0.0002	0.4378	0.0151	0.1240	0.0037	0.0133	0.0004	0.7861	0.0020	163	1	369	13
4	29	335	285	0.8	0.0757	0.0004	0.6919	0.0064	0.0662	0.0006	0.0221	0.0003	471	3	534	5	814	19
5	21	223	241	1.1	0.0762	0.0005	0.8378	0.0172	0.0797	0.0015	0.0220	0.0004	473	3	618	13	1190	36
6	34	698	415	0.6	0.0407	0.0002	0.5743	0.0103	0.1023	0.0017	0.0185	0.0003	257	1	461	8	1666	30
7	43	462	493	1.1	0.0757	0.0004	0.8814	0.0105	0.0845	0.0009	0.0230	0.0004	470	3	642	8	1304	20
8	99	551	1193	2.2	0.0945	0.0006	3.4322	0.0336	0.2634	0.0022	0.0393	0.0007	582	3	1512	15	3267	13
9	141	684	399	0.6	0.1633	0.0009	3.5309	0.0297	0.1568	0.0013	0.0810	0.0014	975	5	1534	13	2422	14
10	38	590	613	1.0	0.0527	0.0003	0.5010	0.0077	0.0690	0.0010	0.0164	0.0003	331	2	412	6	899	31
11	24	287	187	0.7	0.0745	0.0004	0.6682	0.0082	0.0651	0.0008	0.0229	0.0004	463	2	520	6	777	25
12	8	175	348	2.0	0.0265	0.0002	0.7145	0.0133	0.1958	0.0037	0.0105	0.0002	2.0412	0.0040	168	1	547	10
13	58	107	47	0.4	0.5042	0.0029	12.070	0.0618	0.1736	0.0008	0.0899	0.0018	2632	15	2610	13	2593	8
14	120	438	180	0.4	0.2633	0.0014	3.8274	0.0197	0.1054	0.0005	0.0572	0.0012	1507	8	1599	8	1722	9
15	19	52	34	0.7	0.2435	0.0020	7.9545	0.1262	0.2369	0.0031	0.1872	0.0049	1405	11	2226	35	3099	21
16	197	1051	132	0.1	0.1870	0.0010	2.7700	0.0141	0.1075	0.0005	0.0706	0.0020	1105	6	1347	7	1757	9
17	54	550	681	1.2	0.0804	0.0004	0.7030	0.0063	0.0634	0.0006	0.0217	0.0006	499	3	541	5	722	19
18	319	1244	524	0.4	0.2471	0.0013	3.0770	0.0151	0.0903	0.0004	0.0616	0.0015	1424	8	1427	7	1432	9
19	433	1792	765	0.4	0.2351	0.0013	2.9213	0.0145	0.0901	0.0004	0.0517	0.0011	1361	7	1387	7	1428	9
20	255	590	165	0.3	0.4085	0.0026	8.3907	0.0479	0.1490	0.0007	0.1022	0.0023	2208	14	2274	13	2334	8
21	318	717	494	0.7	0.3926	0.0022	7.5638	0.0377	0.1397	0.0006	0.0904	0.0016	2135	12	2181	11	2224	8
22	85	1217	760	0.6	0.0652	0.0004	0.6571	0.0051	0.0731	0.0005	0.0169	0.0003	407	2	513	4	1017	15
23	41	223	92	0.4	0.1777	0.0011	1.8138	0.0125	0.0740	0.0005	0.0500	0.0008	1054	6	1050	7	1043	12
24	23	269	195	0.7	0.0753	0.0005	0.6230	0.0058	0.0600	0.0006	0.0237	0.0004	468	3	492	5	603	22
25	43	928	420	0.5	0.0445	0.0002	0.3446	0.0023	0.0562	0.0004	0.0142	0.0003	280	1	301	2	460	14
26	95	3538	918	0.3	0.0261	0.0002	0.2300	0.0014	0.0639	0.0005	0.0118	0.0002	166	1	210	1	737	16
27	40	1438	820	0.6	0.0257	0.0002	0.1880	0.0016	0.0530	0.0004	0.0082	0.0001	164	1	175	1	331	17
28	16	574	337	0.6	0.0257	0.0001	0.1819	0.0026	0.0514	0.0007	0.0088	0.0001	163	1	170	2	259	33
29	22	772	421	0.5	0.0260	0.0001	0.2182	0.0034	0.0609	0.0010	0.0089	0.0002	165	1	200	3	636	34
30	7	230	163	0.7	0.0265	0.0002	0.2097	0.0095	0.0575	0.0025	0.0090	0.0002	168	1	193	9	511	96
31	65	775	782	1.0	0.0732	0.0004	0.5968	0.0038	0.0591	0.0004	0.0188	0.0003	455	2	475	3	572	13
32	13	79	57	0.7	0.0695	0.0011	4.8398	0.1192	0.5051	0.0077	0.1101	0.0027	433	7	1792	44	4256	23
33	23	254	377	1.5	0.0756	0.0005	0.7425	0.0115	0.0713	0.0010	0.0160	0.0003	470	3	564	9	965	28
35	227	664	283	0.4	0.3299	0.0025	5.8612	0.0317	0.1289	0.0007	0.0500	0.0009	1838	14	1956	11	2083	10

Table 2 continued

Samples Spot no.	Pb (ppm)	U (ppm)	Th (ppm)	Th/U	$^{207}Pb/^{206}Pb$	± 1σ	$^{207}Pb/^{235}U$	± 1σ	$^{206}Pb/^{238}U$	± 1σ	$^{208}Pb/^{232}Th$	± 1σ	$^{206}Pb/^{238}U$		$^{207}Pb/^{235}U$		$^{207}Pb/^{206}Pb$	
													Age (Ma)	± 1σ	Age (Ma)	± 1σ	Age (Ma)	± 1σ
36	349	821	156	0.2	0.4079	0.0025	8.3286	0.0527	0.1481	0.0007	0.1120	0.0020	2206	13	2267	14	2324	8
37	249	1096	231	0.2	0.2147	0.0011	3.7445	0.0180	0.1265	0.0006	0.0950	0.0015	1254	7	1581	8	2049	8
38	8	159	112	0.7	0.0441	0.0003	0.3254	0.0103	0.0535	0.0017	0.0137	0.0002	278	2	286	9	349	70
39	70	2552	1642	0.6	0.0254	0.0001	0.2002	0.0013	0.0573	0.0004	0.0071	0.0001	161	1	185	1	502	15
40	25	343	113	0.3	0.0710	0.0004	0.5785	0.0079	0.0591	0.0008	0.0229	0.0005	442	2	464	6	570	30

zonal structure. The ratios of Th to U of zircons were all bigger than 0.4, reflecting the characteristics of magmatic zircon (Wu and Zheng 2004). However, such a large age range indicated that a lot of zircons in the old crust were captured by later magmatism. In other words, many zircons were the inherited magmatic zircons. Among them, 6 zircons had the youngest and concentrated ages (161–168 Ma) with the weighted average age of 164.3 ± 2.4 Ma (Fig. 9).

5.3 Hf isotopic characteristics

Zircon Hf isotopic data is shown in Table 3. According to the results, 6 zircons with 161–168 Ma had εHf(t) value range from + 7.8 to + 12.1; the model age T_{DM2} of the depleted mantle was between 727 and 1112 Ma. The εHf(t) value of zircon with 268 Ma was + 4.5 and T_{DM} was 747 Ma. The εHf(t) value of zircon with 278 Ma was − 20.6 and T_{DM} was about 1716 Ma. The εHf(t) value of zircon with 442–499 Ma ranged from − 7.5 to + 13.4 and T_{DM} was between 549 and 1395 Ma.

6 Discussions

6.1 Age of granitoid

As mentioned above, among the zircon samples from the granitoid dike in Luodian, there are many inherited zircons whose age peaks correspond to that of detrital zircons in the bauxite stratum in northern Guizhou (Jing et al. 2013; Jin et al. 2013). This indicates the mixing of shallow crust materials. According to the field geology, the granitoid dike in Luodian directly intruded and cut across the diabase. The age of the diabase was 261.9 ± 2.1 Ma, which was close to the age of the xenocrystic zircons from 257 to 280 Ma. This indicates that the formation age of the dike was later than 261.9 Ma. From the zircon dating results of the dike, it has been found that the only zircons with the age of 161–168 Ma were later than 261.9 Ma, they have similar ages, and they have obvious magmatic bands. Their ages could represent the crystallization age of granitoid dike. Moreover, the zircons with ages older than 975 Ma suggest the widespread presence of unexposed Proterozoic and Archean basement in southwest Yangtze craton, which is similar to that of zircons in east Guizhou (Zheng et al. 2006).

6.2 Source of the granitoid

Granitoid in Luodian had high contents of SiO_2 (65.2%–66.8%) and total alkali ($Na_2O + K_2O$: 9.01%–9.95%) and low contents of Mg, Fe, Ca, P and Ti, showing the

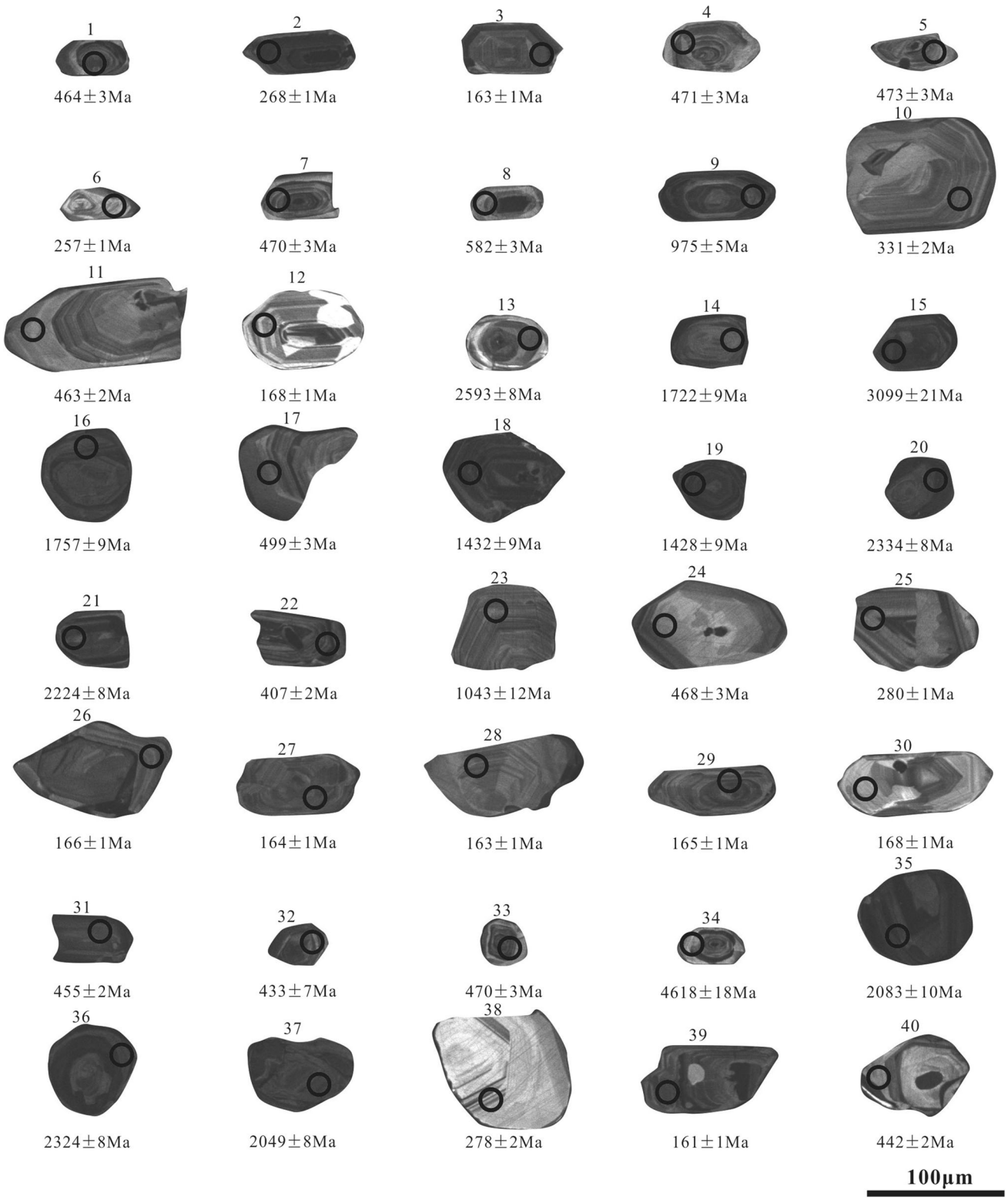

Fig. 8 CL photomicrographs of zircons

characteristics of rich alkali granite (Bi et al. 2000). It had low 10,000 Ga/Al (1.67–1.96) and FeO*/MgO (6.13–7.74), indicating that it had no characteristics of A type granite (Whalen et al. 1987). Its relatively low A/CNK value (0.93) reflects that it had no characteristics of S type granite, either. However, its relatively low P_2O_5 content (0.10%–

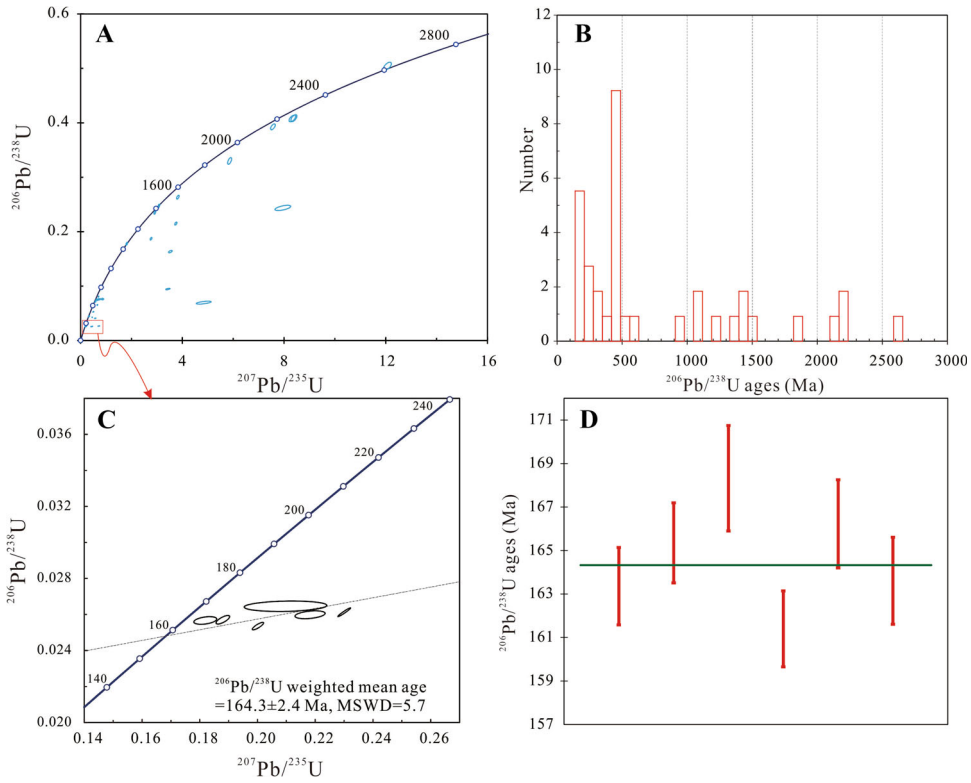

Fig. 9 Zircon U–Pb dating plot of the granitoid. **a** Concordia plot for granitoid; **b** $^{206}Pb/^{238}U$ age column of all zircons of granitoid; **c** concordia plot for ~ 164 Ma of granitoid; **d** $^{206}Pb/^{238}U$ average weighted age diagram of zircons in 164 Ma of granitoid

Table 3 Hf isotope data from zircons of the granitoid

Spot no.	$^{176}Yb/^{177}Hf$	$^{176}Lu/^{177}Hf$	± 1σ	$^{176}Hf/^{177}Hf$	± 1σ	εHf(t)	± 1σ	T_{DM1}	T_{DM2}	t (Ma)
1	0.041373	0.001765	0.000059	0.282867	0.000135	13.0	4.8	557	1232	464
4	0.030781	0.001184	0.000070	0.282869	0.000031	13.4	1.1	546	1223	471
7	0.045788	0.001709	0.000110	0.282799	0.000030	10.8	1.1	655	1443	470
11	0.035207	0.000876	0.000049	0.282822	0.000018	11.7	0.6	609	1366	463
17	0.024209	0.000746	0.000038	0.282257	0.000028	− 7.5	1.0	1395	3153	499
24	0.031347	0.000979	0.000036	0.282303	0.000022	− 6.6	0.8	1340	2999	468
31	0.046905	0.001610	0.000017	0.282626	0.000039	4.4	1.4	901	1966	455
40	0.017937	0.000704	0.000050	0.282672	0.000022	6.0	0.8	816	1807	442
2	0.082237	0.002483	0.000027	0.282746	0.000028	4.5	1.0	747	1619	268
38	0.021677	0.000610	0.000096	0.282021	0.000020	− 20.6	0.7	1716	3869	278
26	0.022629	0.000602	0.000058	0.282973	0.000019	10.7	0.7	392	861	166
27	0.034254	0.000971	0.000012	0.283002	0.000022	11.6	0.8	354	767	164
28	0.019039	0.000498	0.000079	0.283014	0.000023	12.1	0.8	333	727	163
29	0.034795	0.001125	0.000010	0.282986	0.000032	11.1	1.1	378	815	165
30	0.063316	0.001927	0.000034	0.282894	0.000024	7.8	0.8	521	1112	168
39	0.067674	0.002040	0.000034	0.282965	0.000023	10.1	0.8	419	874	161

εHf(t) values are calculated using present-day $(^{176}Lu/^{177}Hf)_{CHUR} = 0.0332$ and $(^{176}Hf/^{177}Hf)_{CHUR} = 0.282772$ (Blichert-Toft and Albarède 1997). T_{DM2} values are calculated using present-day $(^{176}Lu/^{177}Hf)_{DM} = 0.0384$ and $(^{176}Hf/^{177}Hf)_{DM} = 0.28325$ (Griffin et al. 2000). The decay constant of ^{176}Lu is 1.865×10^{-11} $year^{-1}$ (Scherer et al. 2001). $^{176}Hf/^{177}Hf$ value for the average continental crust is 0.015 (Griffin et al. 2002)

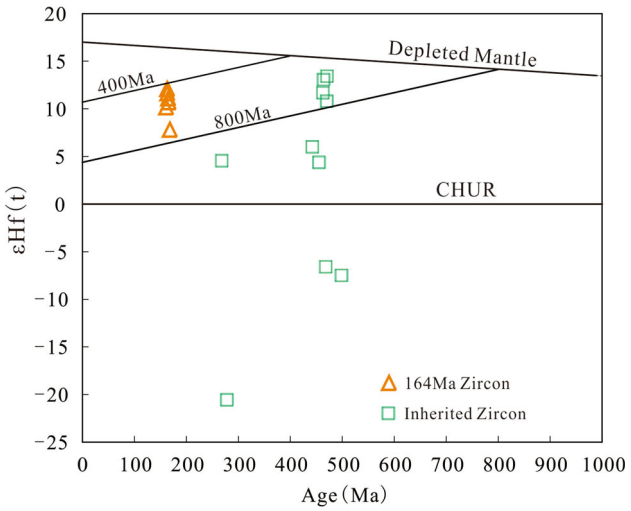

Fig. 10 The relationship between age and εHf(t) of zircons of the granitoid

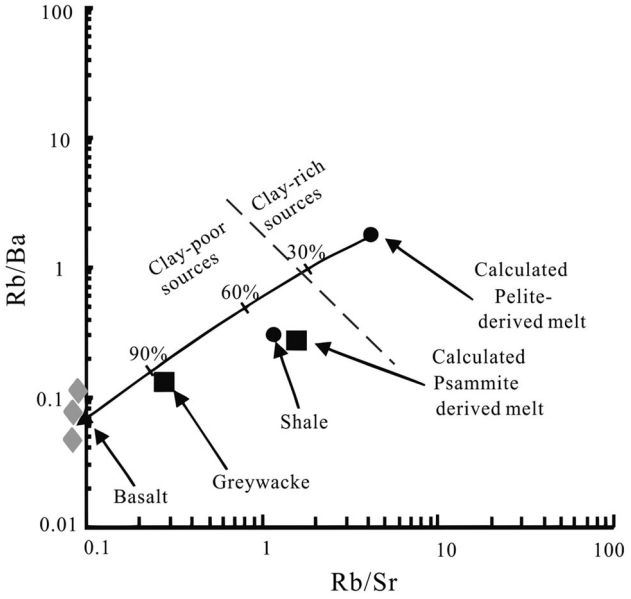

Fig. 11 The Rb/Sr–Rb/Ba diagram of the granitoid (after Sylvester 1998)

0.21%) shows that it has certain characteristics of I-type granite (Chappell and White 1992, 2001).

Six zircons in 161–168 Ma with the εHf(t) from + 7.8 to + 12.1 (Fig. 10) showed that their source rocks mainly derived from the newly grown basaltic crust, and the Rb/Sr–Rb/Ba diagram also shows that the source magma of the gratinoid was from basalt (Fig. 11). The various age peaks of inherited magmatic zircons (257–280 Ma, 407–499 Ma, 975–1105 Ma, 1405–1520 Ma, ~ 1800 Ma, 2135–2280 Ma and ~ 2632 Ma) is the strongest evidence of the adopted petrogenetic model involving crustal contamination, all the inherited zircons were captured during the intrusion of magma. Furthermore, the T_{DM2} model ages (1112–727 Ma) of the granitoid dike indicate a relatively large crustal residence time, which may mean that the large anatexia processes and crustal rework in the southwest Yangtze block. It could be calculated through the Zirconium-saturated thermometer (Watson and Harrison 1983) that the granitoid in Luodian had a high temperature of about 950 °C in crystallization. The high temperature may also indicate that the granitoid may have originated from the partial melting of the mantle or lower crust. Experimental petrological evidence shows that direct partial melting of the mantle peridotite can only form the igneous rock whose silica content was not higher than that of andesite (Baker et al. 1995; Green 1973). Therefore, Luodian granitoid was not solely formed by partial melting of mantle peridotite directly. However, since the basic magma is formed by partial melting of mantle peridotite, this may have produced granite magma after assimilation contamination of crust-derived materials which then experienced strong crystallization and differentiation (Kemp et al. 2007; Li et al. 2009a, b). The granitoid dike in Luodian enriched LILE but depleted HFSE, which also suggests crustal contamination. A large number of xenocrystic zircons have been discovered, indicating its contamination by hypabyssal crustal-derived materials in the diagenetic process. The granitoid dike also had low contents of Fe, Mg, and Ca, suggesting that it experienced strong crystallization differentiation, maybe experiencing the crystallization differentiation of mafic minerals (olivine and pyroxene). It depleted Ti and P, indicating that it may experience the crystallization differentiation of rich titanium minerals and apatite (Zhong et al. 2009).

6.3 Dynamic background and its metallogenic implication

The granitoid intruded as the dike, indicating that it was formed in the stretching environment. The tectonic environment discrimination diagram showed that Luodian granitoid was mainly produced in the intraplate granite area (Fig. 12), indicating that it may have been formed in the stretching environment after intraplate orogeny. The intraplate orogeny stage was accompanied by the mineralization. In this stage, the extrusion tectonics of crust and mantle could lead to the horizontal migration of the ore-bearing fluid, which may be favorable to mineralize at the stress release area (Luo et al. 2007). At the stage of large-scale magmatic activities at the orogenic belt, it is generally unlikely to form large deposits, but at the end of orogenesis or the post-tectonic stretching stage, it is favorable to mineralization (de Boorder et al. 1998). Great mineralization has been developed in the southern Guizhou province (Hu and Zhou 2012), such as Carlin-type Au

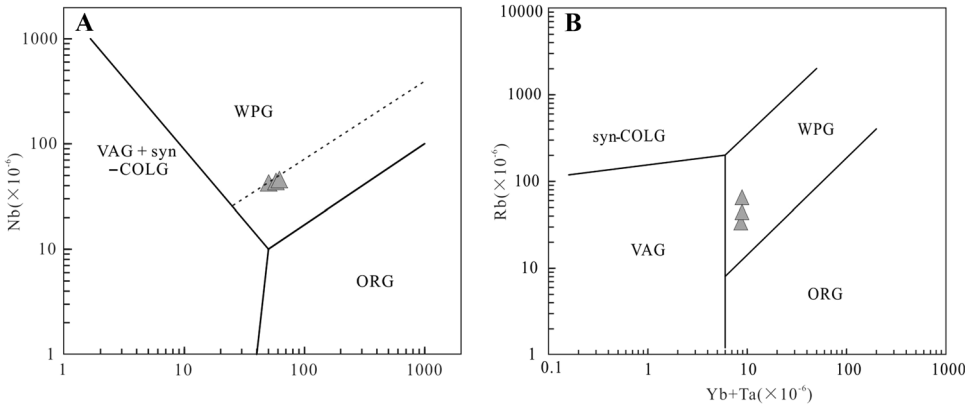

Fig. 12 Tectonic environment diagrams of the granitoid (modified after Pearce et al. 1984). WPG-intraplate granite; VAG-volcanic arc granite; Syn-COLG-Syn-collision granite; ORG-oceanic ridge granite; the dotted line is the boundary line of abnormally ORG

mineralization, whose metallogenic age spans largely from 143 to 193 Ma. Some studies have shown that the mineralization source may be associated with magmatism (Su et al. 2009; Xia et al. 2009; Liu et al. 2017), but there are few reports on Jurassic igneous activities. The granitoid dike in Luodian has very obvious characteristics of mantle-derived lower crust magma, indicating that in the Jurassic period (ca. 164 Ma), intracontinental extension happened in the south of Guizhou, with the intrusion of mantle-derived materials into the shallow crust. This discovery indicates that some mantle-derived materials have risen to the shallow crust through the fault, which provides the possible genesis for the greatly valuable hydrothermal deposits in the southwest of Guizhou in this period and has important significance to re-recognize the magmatic rock-tectonic evolution and mineralization in the south of Guizhou and neighboring areas.

7 Conclusions

1. Zircon U–Pb dating showed that the age of the granitoid dike in Luodian was about 164 Ma.
2. The granitoid dike's concentration of rich alkali granite, its positive εHf(t) value of + 7.8 to + 12.1, and its great number of older inherited zircons, indicates that the granitoid dike was formed from the partial melting of newly grown basaltic crust, and then experienced crustal contamination and strong fractional crystallization.
3. The granitoid belongs to intra-plate origin, which is formed in the post-tectonic stretching stage. It indicates that in this period, a large number of mantle-derived materials rose to the shallow crust, which may contribute to regional mineralization in the south of Guizhou and neighboring areas.

Acknowledgements We sincerely thank Prof. Zhang Zhuru, Prof. Zhang Xinchun and Prof. Su Wenchao for insightful suggestions, Prof. Li Mingqin, Prof. Xie Hong and Dr. Gao Junbo for lab assistance and Dr. Huang Zhiyong and Engineer Hao Jiaxu for the field-work. This research was funded by grants from the National Natural Science Foundation of China (No.41262005), high-level personnel of Guizhou Institute of Technology (No. XJGC20140702) and Talent introduction project of Guizhou University (No. 702400163301).

References

Anderson T (2002) Correction of common lead in U–Pb analyses that do not report ^{204}Pb. Chem Geol 192(1–2):59–79

Baker MB, Hirschmann MM, Ghiorso MS, Stolper EM (1995) Compositions of near-solidus peridotite melts from experiments and thermodynamic calculations. Nature 375(6529):308–311

Bi X, Hu R, Ye Z, Shao S (2000) Relations between A-type granites and copper mineralization as exemplified by the machangqing Cu deposit. Sci China (Series D) 43(1):93–102

Blichert-Toft J, Albarède F (1997) The Lu-Hf isotope geochemistry of chondrites and the evolution of the mantle-crust system. Earth Planet Sci Lett 148(1–2):243–258

Boorder H, Spakman W, White SH, Wortel MJR (1998) Late Cenozoic mineralization, orogenic collapse and slab detachment in the European Alpine Belt. Earth Planet Sci Lett 164(3–4):569–575

Chappell BW, White AJR (1992) I-type and S-type granites in the Lachlan fold belt. Trans R Soc Edinburgh-Earth Sci 83:1–26

Chappell BW, White AJR (2001) Two contrasting granite types: 25 years later. Aust J Earth Sci 48(4):489–499

Chen Y, Sheng Y, Cao G (1994) Regional geological outline in China. Geological Publishing House, Beijing **(in Chinese)**

Chen W, Liu J, Wang Z, Zheng Q (2003) Study on lithofacies palaeogeography during Permian Emeishan basalt explosion in Guizhou Province, China. J Paleogeogr (Chinese Edition) 5(1):17–28 **(in Chinese with English abstract)**

Chen M, Mao J, Qu W, Wu L, Phillip J (2007) Re-Os dating of arsenian pyrites from the Lannigou Gold deposit, Zhenfeng, Guizhou province, and its geological significances. Geol Rev 53(3):371–383 **(in Chinese with English abstract)**

Frost BR, Barnes CG, Collius WJ, Arculus RJ, Ellis DJ, Frost CD (2001) A geochemical classification for granitic rocks. J Petrol 42(11):2033–2048

Geng J, Li H, Zhang J, Zhou H, Li H (2011) Zircon Hf isotope analysis by means of LA-MC-ICP-MS. Geol Bull China 30(10):1508–1513 **(in Chinese with English abstract)**

Geng J, Zhang J, Li H, Li H, Zhang Y, Hao S (2012) Ten-micron-sized zircon U–Pb dating using LA-MC-ICP-MS. Acta Geosci Sin 33(06):877–884 **(in Chinese with English abstract)**

Green D (1973) Experimental melting studies on a model upper mantle composition at high pressure under water-saturated and water-undersaturated conditions. Earth Planet Sci Lett 19(1):37–53

Griffin WL, Pearson NJ, Belousova E, Jackson SE, van Achterbergh E, O'Reilly SY, Shee SR (2000) The Hf isotope composition of cratonic mantle:LAM-MC-ICPMS analysis of zircon megacrysts in kimberlites. Geochim Cosmochim Acta 64(1):133–147

Griffin WL, Wang X, Jackson SE, Pearson NJ, O'Reilly SY, Xu XS, Zhou XM (2002) Zircon chemistry and magma mixing, SE China: in-situ analysis of Hf isotopes Tonglu and Pingtan igneous complexes. Lithos 61(3–4):237–269

Hu R, Zhou M (2012) Multiple Mesozoic mineralization events in South China-an introduction to the thematic issue. Mineralium Deposita 47(6):579–588

Jin Z, Zhou J, Huang Z, Gu J, Liu L, Dai L (2013) Detrital zirxon U–Pb dating and its geological significance for the bauxite in Wuchuan-Zheng'an-Daozhen Al metallogenic province, Guizhou, SW China. Earth Sci Front 06:226–239 **(in Chinese with English abstract)**

Gu J, Huang Z, Fan H, Ye L, Jin Z (2013) Provenance of lateritic bauxite deposits in the Wuchuan–Zheng'an–Daozhen area, Northern Guizhou Province, China: LA-ICP-MS and SIMS U–Pb dating of detrital zircons. J Asian Earth Sci 70–71:265–282

Kemp AIS, Hawkesworth CJ, Foster GL, Paterson BA, Woodhead JD, Hergt JM, Gray CM, Whitehouse MJ (2007) Magmatic and crustal differentiation history of granitic rocks from Hf-O isotopes in zircon. Science 315(5814):980–983

Li H, Lu S, Li H, Sun L, Xiang Z, Geng J, Zhou H (2009a) Zircon and beddeleyite U–Pb precision dating of basic rock sills intruding Xiamaling Formation. North China. Geol Bull China 28(10):1396–1404 **(in Chinese with English abstract)**

Li J, Zhao X, Zhou M, Ma C, de Souza Z, Vasconcelos P (2009b) Late Mesozoic magmatism from the Daye region, eastern China: U–Pb ages, petrogenesis, and geodynamic implications. Contrib Mineral Petrol 157(3):383–409

Liu Y, Hu Z, Zong K, Gao C, Gao S, Xu J, Chen H (2010) Reappraisement and refinement of zircon U–Pb isotope and trace element analyses by LA-ICP-MS. Chin Sci Bull 55(15):1535–1546

Liu J, Li J, Zhou Z, Wang Z, Chen F, Deng L, Yang C, Hou L, Jin X, Li J, Yang B, Xu L, Zhang M, Zhang J, Zhang L, Li S, Long C, Fu Z, He Y, Meng M, Wang X (2017) New progress of exploration and research of Zhenfeng-Puan gold fully equipped exploration area. Guizhou Geology 34(4):244–254 **(in Chinese with English abstract)**

Ludwing KR (2001) Users manual for Isoplot/Ex(rev.2.49): a geochronological toolkit for Microsoft Excel. Berkeley Geochronology Center, Special Publication, 1a, 55

Luo Z, Liang T, Chen B, Xin H, He S, Zhang Z, Cheng S (2007) Intraplate orogenesis and its implication in metallogenesis. Acta Petroligica Sinica 23(8):1945–1956 **(in Chinese with English abstract)**

Maniar PD, Piccoli PM (1989) Tectonic discrimination of granitoids. Geol Soc Am Bull 101(5):635–643

McDonough WF, Sun SS (1995) The composition of the Earth. Chem Geol 120(3–4):223–253

Middlemost EAK (1994) Naming materials in the magma/igneous rock system. Earth Sci Rev 37(3–4):215–224

Pearce JA, Harris NBW, Tindle AG (1984) Trace element discrimination diagrams for the tectonic inter pretation of granitic rocks. J Petrol 25(4):956–983

Peccerillo R, Taylor SR (1976) Geochemistry of eocene calc-alkaline volcanic rocks from the Kastamonu area, Northern Turkey. Contrib Miner Petrol 58(1):63–81

Scherer E, Münker C, Mezger K (2001) Calibration of the lutetium-hafnium clock. Science 293(5530):683–687

Shu L (2006) Predevonian tectonic evolution of south China: from Cathaysian block to Caledonian Period folded orogenic belt. Geol J China Univ 12(4):418–431

Su W, Heinrich CA, Pettke T, Zhang X, Hu R, Xia B (2009) Sediment-hosted gold deposits in Guizhou, China: products of Wall-Rock sulfidation by deep crustal fluids. Econ Geol 104(1):73–93

Su WC, Dong WD, Zhang XC, Shen NP, Hu RZ, Hofstra AH, Cheng LZ, Xia Y, Yang KY (2018) Carlin-type gold deposits in the Dian-Qian-Gui "Golden Triangle" of southwest China. Rev Econ Geol 20:157–185

Sun SS, McDonough WF (1989) Chemical and isotopic systematics of oceanic basalts: implications for mantle composition and processes. In: Saunders AD, Norry MJ (eds) Magmatism in the Oceanic Basins. Special Publication of Geological Society of London, vol 42, pp 313–345

Sylvester PJ (1998) Post-collisional strongly peraluminous granites. Lithos 45(1–4):29–44

Wang Z, Kuang G (1997) Characteristics of the Late Paleozoic Oceanic Basalts and their eruptive enrivonments in West Guangxi. Acta Petroligica Sinica 13(02):135–140 **(in Chinese with English abstract)**

Watson EB, Harrison TM (1983) Zircon saturation revisited: temperature and composition effects in a variety of crustal magma types. Earth Planet Sci Lett 64(2):295–304

Whalen JB, Currie KL, Chappell BW (1987) A-type granites: geochemical characteristics, discrimination and petrogenesis. Contrib Miner Petrol 95(4):407–419

Wu Y, Zheng Y (2004) The study on the genetic mineralogy of zircon and its constraint of the interpretation of U–Pb age. Chin Sci Bull 49(16):1589–1604 **(in Chinese)**

Wu H, Kuang G, Wang Z (1993) Reinterpretation of basic igneous rocks in Western Guanxi and its tectonic implications. Chin J Geol 28(03):288–289 **(in Chinese with English abstract)**

Wu H, Kuang G, Wang Z (1997a) Preliminary study on Late Paleozoic Tectonic sedimentary settings in Guanxi. Chin J Geol 32(01):11–18 **(in Chinese with English abstract)**

Wu X, Wu H, Li S (1997b) Geotectonic setting of regional mineralization on the Southwestern margin of the Yangtze Terrain and tectonic-constraints on the formation of ore deposits. Acta Mineralogica Sinica 17(4):376–385 **(in Chinese with English abstract)**

Xia Y, Zhang Y, Su W, Tao Y, Zhang X, Liu J, Deng Y (2009) Metallogenic model and prognosis of the Shuiyindong super-large stratabound Carlin-type gold deposit, Southwestern Guizhou province, China. Acta Geologica Sinica 83(10):1473–1482 **(in Chinese with English abstract)**

Xie ZJ, Xia Y, Cline JS, Koenig A, Wei DT, Tan QP, Wang ZP (2018) Are there Carlin-type gold deposits in China? A comparison of the Guizhou, China, deposits and Nevada, USA, deposits. Rev Econ Geol 20:187–233

Xu Y, Chuang S, Jahn B, Wu G (2001) Petrologic and geochemical constraints on the petrogenesis of Permian-Triassic Emeishan flood basalts in southwestern China. Lithos 58(3–4):145–168

Zhang Q, Qian Q, Wang Y, Xu P, Han S, Jiu X (1999) Late Paleozoic basic magmatism from SW Yangtze Massif and evolution of the Paleo-Tethyan Ocean. Acta Petrologica Sinica 15(04):576–583 **(in Chinese with English abstract)**

Zheng L (2017) The mineralization and mineralization of the Nibao gold deposit in southwest Guizhou. Doctoral dissertation, Guizhou University

Zheng J, Griffin WL, O'Reilly SY, Zhang M, Pearson N (2006) Widespread Archean basement beneath the Yangtze Craton. Geology 34(6):417–420

Zhong H, Zhu W, Hu R, Xie L, He D, Liu F, Chu Z (2009) Zircon U–Pb age and Sr-Nd-Hf isotope geochemistry of the Panzhihua A-type syenitic intrusion in the Emeishan large igneous province, southwest China and implications for growth of juvenile crust. Lithos 110(1–4):109–128

Zhu M, Tian Y, Nie A, Zhang H, Yang H (2018) Petrogeochemistry, zircon SHRIMP U–Pb geochronology of Mafic Dykes in Southern Guizhou and their geological implications. J Earth Sci 43(04):1333–1349 **(in Chinese with English abstract)**